Monthly Notices
of the
ROYAL ASTRONOMICAL SOCIETY

MNRAS **434,** 1300–1308 (2013) doi:10.1093/mnras/stt1089
Advance Access publication 2013 July 11

High-precision photometry by telescope defocusing – V. WASP-15 and WASP-16*

John Southworth,[1]† L. Mancini,[2,3] P. Browne,[4] M. Burgdorf,[5] S. Calchi Novati,[3,6] M. Dominik,[4]‡ T. Gerner,[7] T. C. Hinse,[8] U. G. Jørgensen,[9,10] N. Kains,[11] D. Ricci,[12] S. Schäfer,[13] F. Schönebeck,[7] J. Tregloan-Reed,[1] K. A. Alsubai,[14] V. Bozza,[3,15] G. Chen,[2,16] P. Dodds,[4] S. Dreizler,[13] X.-S. Fang,[17] F. Finet,[18] S.-H. Gu,[17] S. Hardis,[9,10] K. Harpsøe,[9,10] Th. Henning,[2] M. Hundertmark,[4] J. Jessen-Hansen,[19] E. Kerins,[20] H. Kjeldsen,[19] C. Liebig,[4] M. N. Lund,[19] M. Lundkvist,[19] M. Mathiasen,[9,10] N. Nikolov,[2,21] M. T. Penny,[22] S. Proft,[7] S. Rahvar,[23] K. Sahu,[24] G. Scarpetta,[3,6,15] J. Skottfelt,[9,10] C. Snodgrass,[25] J. Surdej[17] and O. Wertz[17]

[1]*Astrophysics Group, Keele University, Staffordshire ST5 5BG, UK*
[2]*Max Planck Institute for Astronomy, Königstuhl 17, D-69117 Heidelberg, Germany*
[3]*Dipartimento di Fisica 'E. R. Caianiello', Università di Salerno, Via Ponte Don Melillo, I-84084-Fisciano (SA), Italy*
[4]*SUPA, University of St Andrews, School of Physics & Astronomy, North Haugh, St Andrews KY16 9SS, UK*
[5]*HE Space Operations GmbH, Flughafenallee 24, D-28199 Bremen, Germany*
[6]*Istituto Internazionale per gli Alti Studi Scientifici (IIASS), I-84019 Vietri Sul Mare (SA), Italy*
[7]*Zentrum für Astronomie, Universität Heidelberg, Mönchhofstraße 12-14, D-69120 Heidelberg, Germany*
[8]*Korea Astronomy and Space Science Institute, Daejeon 305-348, Republic of Korea*
[9]*Niels Bohr Institute, Københavns Universitet, Juliane Maries vej 30, DK-2100 Copenhagen Ø, Denmark*
[10]*Centre for Star and Planet Formation, Natural History Museum of Denmark, Københavns Universitet, Øster Voldgade 5-7, DK-1350 København K, Denmark*
[11]*European Southern Observatory, Karl-Schwarzschild-Straße 2, D-85748 Garching bei München, Germany*
[12]*Instituto de Astronomía-UNAM, Km 103 Carretera Tijuana Ensenada, 422860 Ensenada (Baja Cfa), Mexico*
[13]*Institut für Astrophysik, Georg-August-Universität Göttingen, Friedrich-Hund-Platz 1, D-37077 Göttingen, Germany*
[14]*Qatar Foundation, PO Box 5825, Doha, Qatar*
[15]*Istituto Nazionale di Fisica Nucleare, Sezione di Napoli, I-80126, Napoli, Italy*
[16]*Purple Mountain Observatory & Key Laboratory for Radio Astronomy, Chinese Academy of Sciences, 2 West Beijing Road, Nanjing 210008, China*
[17]*National Astronomical Observatories/Yunnan Observatory, Chinese Academy of Sciences, Kunming 650011, China*
[18]*Institut d'Astrophysique et de Géophysique, Université de Liège, B-4000 Liège, Belgium*
[19]*Stellar Astrophysics Centre (SAC), Department of Physics and Astronomy, Aarhus University, Ny Munkegade 120, DK-8000 Aarhus C, Denmark*
[20]*Jodrell Bank Centre for Astrophysics, University of Manchester, Oxford Road, Manchester M13 9PL, UK*
[21]*Astrophysics Group, University of Exeter, Stocker Road, EX4 4QL Exeter, UK*
[22]*Department of Astronomy, Ohio State University, 140 W. 18th Avenue, Columbus, OH 43210, USA*
[23]*Department of Physics, Sharif University of Technology, PO Box 11155-9161, Tehran, Iran*
[24]*Space Telescope Science Institute, 3700 San Martin Drive, Baltimore, MD 21218, USA*
[25]*Max-Planck-Institute for Solar System Research, Max-Planck Str. 2, D-37191 Katlenburg-Lindau, Germany*

Accepted 2013 June 14. Received 2013 June 13; in original form 2013 April 9

ABSTRACT

We present new photometric observations of WASP-15 and WASP-16, two transiting extrasolar planetary systems with measured orbital obliquities but without photometric follow-up since their discovery papers. Our new data for WASP-15 comprise observations of one transit simultaneously in four optical passbands using GROND on the MPG/European Southern Observatory (ESO) 2.2 m telescope, plus coverage of half a transit from DFOSC on the Danish 1.54 m telescope, both at ESO La Silla. For WASP-16 we present observations of four

* Based on data collected with the Gamma Ray Burst Optical and Near-Infrared Detector (GROND) at the MPG/ESO 2.2 m telescope and by MiNDSTEp with the Danish 1.54 m telescope at the ESO La Silla Observatory.

† E-mail: astro.js@keele.ac.uk
‡ Royal Society University Research Fellow.

complete transits, all from the Danish telescope. We use these new data to refine the measured physical properties and orbital ephemerides of the two systems. Whilst our results are close to the originally determined values for WASP-15, we find that the star and planet in the WASP-16 system are both larger and less massive than previously thought.

Key words: stars: fundamental parameters – stars: individual: WASP-15 – stars: individual: WASP-16 – planetary systems.

1 INTRODUCTION

The number of known transiting extrasolar planets (TEPs) is rapidly increasing and currently stands at 310.[1] Their diversity is also escalating: the radius of the largest known example is 40 times greater than that of the smallest. There is a variation of over three orders of magnitude in their masses, excluding those without mass measurements and those which are arguably brown dwarfs. Whilst a small subset of this population has been extensively investigated, the characterization of the majority is limited to the modest photometry and spectroscopy presented in their discovery papers.

The bottleneck in our understanding of the physical properties of most TEPs is the quality of the available transit light curves, which are of fundamental importance for measuring the stellar density and the ratio of the radius of the planet to that of the star. Additional contributions, which arise from the spectroscopic parameters of the host star and the constraints on its physical properties from theoretical models, are usually dwarfed by the uncertainties in the photometric parameters derived from the light curves.

We are therefore undertaking a project aimed at characterizing TEPs visible from the Southern hemisphere (see Southworth et al. 2012b, and references therein), by obtaining high-precision light curves of their transits. We use the telescope defocusing technique, discussed in detail in Southworth et al. (2009a), to collect photometric measurements with very low levels of Poisson and correlated noise. This method is able to achieve light curves of remarkable precision (e.g. Tregloan-Reed & Southworth 2012). In this work we present new observations and determinations of the physical properties of WASP-15 and WASP-16, based on nine light curves covering six transits in total.

1.1 Case history

WASP-15 was identified as a TEP by West et al. (2009), who found it to be a low-density object ($\rho_2 = 0.186 \pm 0.026\,\rho_{\rm Jup}$) orbiting a slightly evolved and comparatively hot host star ($T_{\rm eff} = 6300 \pm 100$ K). Other measurements of the effective temperature of the host star have been made by Maxted, Koen & Smalley (2011), who found $T_{\rm eff} = 6210 \pm 60$ K from the infrared flux method (Blackwell, Petford & Shallis 1980), and by Doyle et al. (2013), whose detailed spectroscopic analysis yielded $T_{\rm eff} = 6405 \pm 80$ K.

Triaud et al. (2010) observed the Rossiter–McLaughlin effect for WASP-15 and found the system to exhibit significant obliquity: the sky-projected angle between the rotational axis of the host star and the orbital axis of the planet is $\lambda = 139.6^{+4.3}_{-5.2}$ degrees. This is consistent with previous findings that misaligned planets are found only around hotter stars (Winn et al. 2010), although tidal effects act to align them over time (Triaud 2011; Albrecht et al. 2012).

The discovery of the planetary nature of WASP-16 was made by Lister et al. (2009), who characterized it as a Jupiter-like planet orbiting a star similar to our Sun. Maxted et al. (2011) and Doyle et al. (2013) measured the host star's $T_{\rm eff}$ to be 5550 ± 60 K and 5630 ± 70 K, respectively, in mutual agreement and a little cooler than the value of 5700 ± 150 K found in the discovery paper.

Observations of the Rossiter–McLaughlin effect for WASP-16 have yielded obliquities consistent with zero: Brown et al. (2012) measured $\lambda = 11^{+26}_{-19}$ degrees and Albrecht et al. (2012) found $\lambda = -4^{+11}_{-14}$ degrees. The large uncertainties in these assessments are due to the low rotational velocity of the star, which results in a small amplitude for the Rossiter–McLaughlin effect.

The physical properties of both systems were comparatively ill-defined, as they rested on few dedicated follow-up light curves: only one light curve in the case of WASP-16 and two data sets afflicted with correlated noise in the case of WASP-15. All three data sets were obtained using EulerCam on the 1.2 m Swiss Euler telescope at European Southern Observatory (ESO) La Silla. In this work we present the first follow-up photometry since the discovery paper for both systems, totalling nine new light curves covering six transits. This new material has allowed us to significantly improve the precision of the measured physical properties. Our analysis also benefited from refined constraints on the atmospheric characteristics of the host stars, as discussed above.

2 OBSERVATIONS AND DATA REDUCTION

We observed one transit of WASP-15 on the night of 2012 January 19 using the GROND instrument mounted on the MPG/ESO 2.2 m telescope at La Silla, Chile. The field of view of this instrument is $5.4' \times 5.4'$ at a plate scale of $0.158''$ pixel^{-1}. Observations were obtained simultaneously in the g, r, i and z passbands and covered a full transit plus significant time intervals before ingress and after egress. CCD readout occurred in slow mode. The telescope was defocused and we autoguided throughout the observations. The moon was below the horizon during the observing sequence. An observing log is given in Table 1.

The data were reduced with the IDL[2] pipeline described by Southworth et al. (2009a), which uses the DAOPHOT package (Stetson 1987) to perform aperture photometry with the APER[3] routine. The apertures were placed by hand and the stars were tracked by cross-correlating each image against a reference image. We tried a wide range of aperture sizes and retained those which gave photometry with the lowest scatter compared to a fitted model. In line with previous experience, we found that the shape of the light curve is very insensitive to the aperture sizes.

[1] Data taken from the Transiting Extrasolar Planet Catalogue (TEPCat) available at http://www.astro.keele.ac.uk/jkt/tepcat/.

[2] The acronym IDL stands for Interactive Data Language and is a trademark of ITT Visual Information Solutions. For further details, see http://www.ittvis.com/ProductServices/IDL.aspx.

[3] APER is part of the ASTROLIB subroutine library distributed by NASA. For further details, see http://idlastro.gsfc.nasa.gov/.

Table 1. Log of the observations presented in this work. N_{obs} is the number of observations, T_{exp} is the exposure time, T_{obs} is the observational cadence and 'Moon illum.' is the fractional illumination of the Moon at the mid-point of the transit.

Transit	Date of first obs.	Start time (UT)	End time (UT)	N_{obs}	T_{exp} (s)	T_{obs} (s)	Filter	Airmass	Moon illum.	Aperture radii (pixel)	Scatter (mmag)
WASP-15											
DFOSC	2010 06 09	23:09	03:09	92	120	155	Bessell *R*	1.15 → 1.00 → 1.08	0.068	32, 45, 70	0.492
GROND	2012 04 19	02:23	09:39	229	62–45	115	Gunn *g*	1.17 → 1.00 → 2.09	0.040	50, 75, 95	0.640
GROND	2012 04 19	02:23	09:39	228	62–45	115	Gunn *r*	1.17 → 1.00 → 2.09	0.040	50, 75, 95	0.481
GROND	2012 04 19	02:23	09:39	225	62–45	115	Gunn *i*	1.17 → 1.00 → 2.09	0.040	50, 75, 100	0.607
GROND	2012 04 19	02:23	09:39	227	62–45	115	Gunn *z*	1.17 → 1.00 → 2.09	0.040	50, 75, 100	0.725
WASP-16											
DFOSC	2010 05 10	01:33	06:17	131	100	128	Bessell *R*	1.18 → 1.01 → 1.22	0.156	30, 50, 80	0.542
DFOSC	2010 06 28	23:25	04:10	136	75	102	Bessell *R*	1.05 → 1.01 → 1.55	0.937	30, 40, 60	1.294
DFOSC	2011 05 13	01:07	05:42	140	90	118	Bessell *R*	1.23 → 1.01 → 1.15	0.752	26, 40, 60	0.586
DFOSC	2011 07 01	23:18	04:36	160	90	120	Bessell *R*	1.05 → 1.01 → 1.88	0.006	34, 45, 70	0.670

We calculated differential-photometry light curves of our target star by combining all good comparison stars into an ensemble with weights optimized to minimize the scatter of the observations taken outside transit. We rectified the data to a zero-magnitude baseline by subtracting a second-order polynomial whose coefficients were optimized simultaneously with the weights of the comparison stars. The effect of this normalization was subsequently taken into account when modelling the data. The final GROND optical light curves are shown in Fig. 1. Our time stamps were converted to the BJD(TDB) time-scale (Eastman, Siverd & Gaudi 2010).

We also used GROND to obtain photometry in the *J*, *H* and *K* passbands simultaneously with the optical observations. The field of view of the GROND near-infrared channels is 10′ × 10′ at a plate scale of 0.60″ pixel^{-1}. These were reduced following standard techniques and with trying multiple alternative approaches to decorrelate the data against airmass and centroid position of the target star. We were unable to obtain good light curves from these data, and suspect that this is because the brightness of WASP-15 pushed the pixel count rates into the non-linear regime, causing the systematic noise which is obvious in Fig. 2.

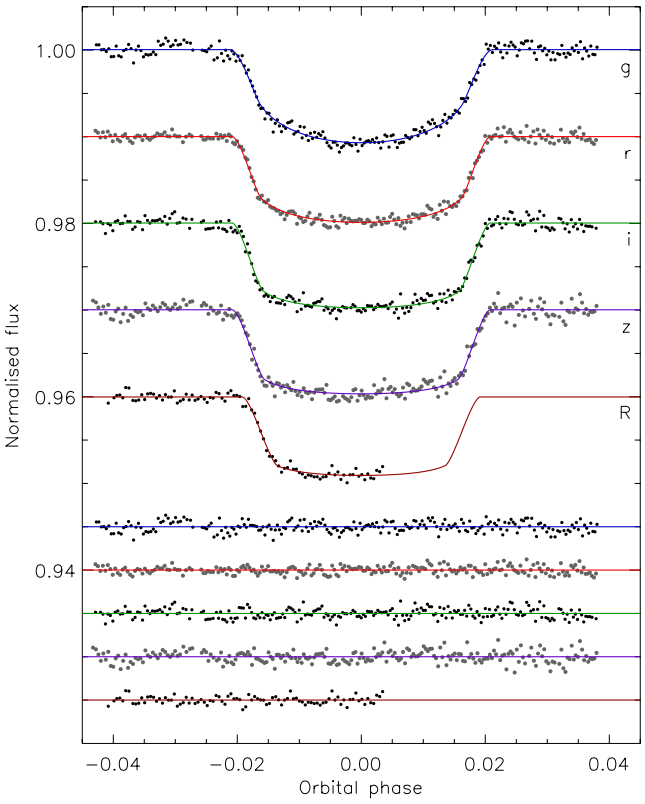

Figure 1. Optical light curves of WASP-15. The first four are from GROND and the fifth is from DFOSC. The JKTEBOP best fit is shown for each data set, and the residuals of the fit are plotted near the base of the figure.

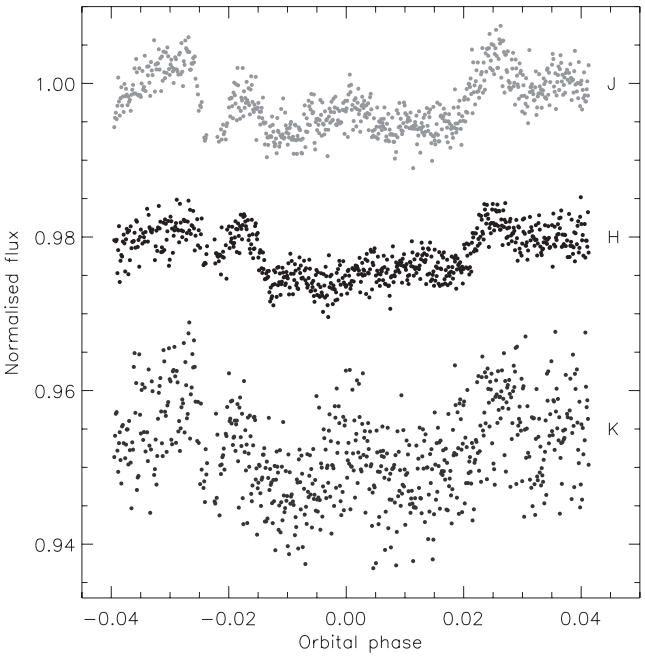

Figure 2. Near-IR light curves of WASP-15 from GROND. The passbands are labelled on the right-hand side of the figure.

A transit of WASP-15 was also observed using the DFOSC imager on-board the 1.54 m Danish telescope at La Silla, which has a field of view of 13.7′ × 13.7′ and a plate scale of 0.39″ pixel^{-1}. We defocused the telescope and autoguided. Several images were taken prior to the main body of observations in order to check for faint nearby stars which might contaminate the point spread function (PSF) of our target star, and none was found. Unfortunately, high winds forced the closure of the dome shortly after the mid-point of the transit, which has limited the usefulness of these data. The data were reduced as above, except that a first-order polynomial (i.e. a straight line) was used as the function to rectify the light curve to zero differential magnitude.

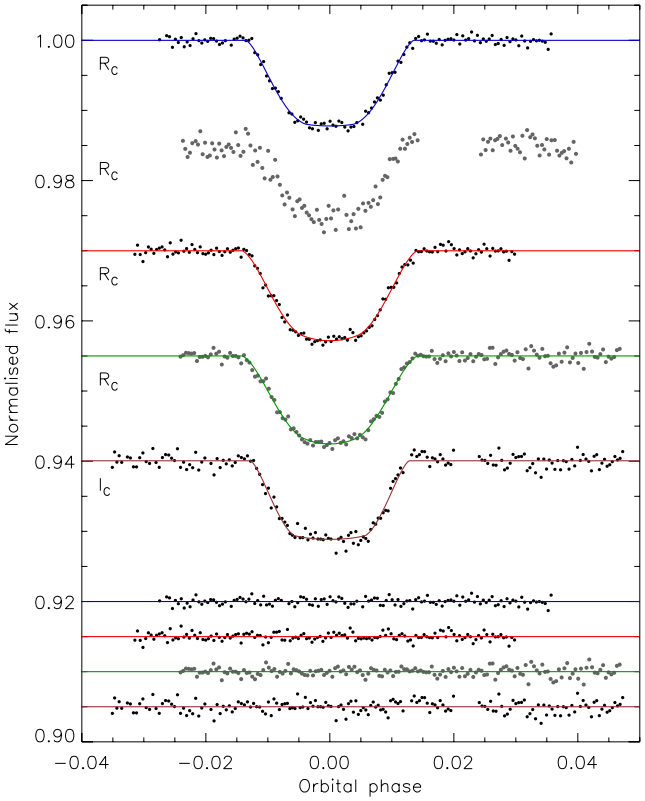

Figure 3. The four new light curves of WASP-16, plotted in the order they are given in Table 1, plus a fifth data set (lower curve) from Lister et al. (2009). The second data set is unreliable and a fitted model is not plotted for it. The JKTEBOP best fits for the other data sets are shown as solid lines and the residuals of the fits are plotted near the base of the figure.

Four transits of WASP-16 were obtained using the DFOSC imager and the same approach as for the WASP-15 transit above. Three of the transits were observed in excellent weather conditions whilst the moon was below the horizon, and these yield excellent light curves. The data were reduced as above, using a straight-line fit to the out-of-transit data. A small number of images taken in focus showed that there are faint stars separated by 32 and 45 pixels from the centre of the PSF of WASP-16. They are fainter than our target star by more than 8.7 and 6.8 mag, respectively, so have a negligible effect on our results.

The second transit was undermined by non-photometric conditions, bright moonlight and a computer crash shortly after the transit finished. This transit is shallower than the other three, and we attribute this to a count rate during the observing sequence that became sufficiently high to enter the regime of significant non-linearity in the CCD response. The data for this transit were not included in subsequent analyses. All four light curves are shown in Fig. 3, along with the Euler telescope data from Lister et al. (2009). All our reduced data will be made available at the CDS.[4]

3 LIGHT-CURVE ANALYSIS

The analysis of our light curves was performed using the *Homogeneous Studies* methodology (see Southworth 2012, and references therein). The light curves were modelled using the JKTEBOP[5] code (Southworth, Maxted & Smalley 2004), which represents the star and planet as biaxial spheroids. The main parameters of the model are the fractional radii of the star and planet, r_A and r_b, and the orbital inclination, i. The fractional radii are the true radii of the objects divided by the orbital semimajor axis. They were parametrized by their sum and ratio:

$$r_A + r_b \qquad k = \frac{r_b}{r_A} = \frac{R_b}{R_A}$$

as the latter are less strongly correlated than the fractional radii themselves.

3.1 Orbital period determination

Our first step was to obtain refined orbital ephemerides. Each of our transit light curves was fitted individually and their error bars rescaled to give $\chi^2_\nu = 1.0$ versus the fitted model. This is needed as the uncertainties from the APER photometry algorithm tend to be underestimated. We then fitted the revised data sets and ran Monte Carlo simulations to measure the transit mid-points with robust error bars.

Our own times of transit mid-point were supplemented with those from the discovery papers (Lister et al. 2009; West et al. 2009). The reference times of transit (T_0) from these papers are given on the BJD and HJD time conventions, respectively, but the time-scales these refer to are not specified (see Eastman et al. 2010). D. R. Anderson (private communication) has confirmed that the time-scales used in these, and the other early WASP planet discovery papers, are UTC. We therefore converted the timings to TDB.

We also compiled publicly available measurements from the Exoplanet Transit Database (ETD[6]), which makes available data sets from amateur observers affiliated with TRESCA.[7] We retained only those timing measurements based on light curves where all four contact points of the transit are easily identifiable. We assumed that the times were all on the UTC time-scales and converted them to TDB for congruency with our own data.

Once the available times of mid-transit had been assembled, we fitted them with straight lines to determine new orbital ephemerides. Table 2 reports all times of mid-transit used for both objects, plus the residuals versus a linear ephemeris. The new ephemeris for WASP-15 is given as

$$T_0 = \mathrm{BJD(TDB)}\ 2454\,584.698\,59(29) + 3.752\,097\,48(81)E,$$

where E represents the cycle count with respect to the reference epoch and the bracketed quantities show the uncertainty in the final digit of the preceding number. The reduced χ^2 of the fit to the timings is encouragingly small at $\chi^2_\nu = 0.78$ for 4 degrees of freedom, which suggests that the orbital period is constant and the uncertainties of the available times of minimum are reasonable. A plot of the fit is shown in Fig. 4.

The situation for WASP-16 is less favourable, with $\chi^2_\nu = 2.59$ (9 degrees of freedom) and large residuals for several of the most precise data points (Fig. 5). We have reason to be cautious about our

[4] http://vizier.u-strasbg.fr/

[5] JKTEBOP is written in FORTRAN77 and the source code is available at http://www.astro.keele.ac.uk/jkt/codes/jktebop.html.

[6] The Exoplanet Transit Database (ETD) can be found at http://var2.astro.cz/ETD/credit.php.

[7] The TRansiting ExoplanetS and CAndidates (TRESCA) website can be found at http://var2.astro.cz/EN/tresca/index.php.

Table 2. Times of minimum light of WASP-15 (upper) and WASP-16 (lower) and their residuals versus the ephemerides derived in this work.

Time of minimum [BJD(TDB) − 2400000]	Cycle number	Residual (JD)	Reference
54 584.698 60 ± 0.000 29	0.0	0.000 01	1
55 320.109 14 ± 0.001 35	196.0	−0.000 55	2
56 036.759 90 ± 0.000 28	387.0	−0.000 42	3 (*g*)
56 036.760 49 ± 0.000 19	387.0	0.000 17	3 (*r*)
56 036.760 44 ± 0.000 23	387.0	0.000 12	3 (*i*)
56 036.760 20 ± 0.000 28	387.0	−0.000 12	3 (*z*)
54 584.429 15 ± 0.000 29	0.0	0.000 17	4
55 276.759 11 ± 0.000 36	222.0	−0.000 57	5
55 311.068 59 ± 0.001 85	233.0	0.004 24	2
55 314.183 58 ± 0.001 00	234.0	0.000 62	2
55 326.657 93 ± 0.000 19	238.0	0.000 54	3
55 376.554 53 ± 0.000 49	254.0	−0.000 56	3
55 688.416 29 ± 0.001 77	354.0	0.000 52	6
55 694.651 94 ± 0.000 20	356.0	−0.001 04	3
55 744.550 44 ± 0.000 23	372.0	−0.000 25	3
56 037.700 89 ± 0.000 24	466.0	0.001 17	7
56 087.595 54 ± 0.001 02	482.0	−0.001 89	8

References: (1) West et al. (2009); (2) T. G.Tan (ETD); (3) This work; (4) Lister et al. (2009); (5) E. Fernandez-Lajus, Y. Miguel, A. Fortier & R. Di Sisto (TRESCA); (6) M. Vrašťák (TRESCA); (7) M. Schneiter, C. Colazo & P. Guzzo (TRESCA); and (8) F. Tifner (TRESCA).

own timings, as the DFOSC time stamps are known to have been incorrect for the 2009 season (Southworth et al. 2009b). This issue was minimized for the 2010 season (which contains the first two transits of WASP-16 we observed) and fixed for the 2011 season (which contains the third and fourth WASP-16 transits), so the disagreement between the two 2011 transits cannot currently be dismissed as an instrumental effect. WASP-16 should be monitored in the future to investigate the possibility that it undergoes transit timing variations. In the meantime, the linear ephemeris given by the timings in Table 2 is

$$T_0 = \mathrm{BJD(TDB)}\ 2454\,584.428\,98(38) + 3.118\,6068(12)E,$$

where the error bars have been multiplied by $\sqrt{2.59}$ to account for the large χ^2_ν.

3.2 Light-curve modelling

We modelled each of our light curves of WASP-15 and WASP-16 individually, using JKTEBOP to fit for $r_\mathrm{A} + r_\mathrm{b}$, k, i and T_0. The best-fitting models are shown in Figs 1 and 3. This individual approach was necessary to allow for differing amounts of limb darkening (LD) for WASP-15 and for possible timing variations in WASP-16, and has the advantage of providing an opportunity to assess error bars by comparing multiple independent sets of results rather than relying on statistical algorithms. The DFOSC transit for WASP-15 lacks coverage of the egress phases so was modelled with T_0 fixed at the value predicted by the orbital ephemeris, and the second transit of WASP-16 was ignored due to the systematic errors discussed in Section 2. The follow-up photometry for WASP-15 presented by West et al. (2009) was not considered as it contains substantial red noise. The Euler telescope light curve of WASP-16 (Lister et al. 2009) was added to our analysis as it has full coverage of a transit event with reasonably high precision.

Light-curve models were obtained using each of five LD laws (see Southworth 2008), with the linear coefficients either fixed at

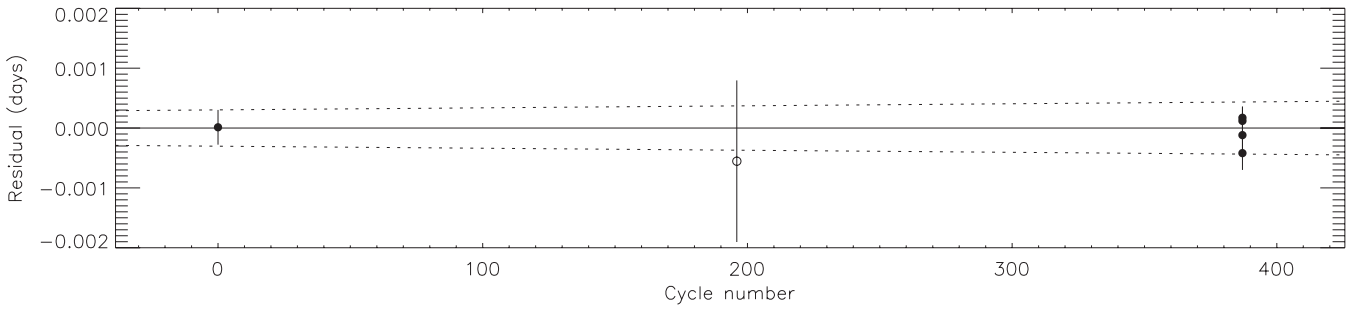

Figure 4. Plot of the residuals of the timings of mid-transit of WASP-15 versus a linear ephemeris. Timings obtained from amateur observations are plotted using open circles, and other timings are plotted with filled circles. The dotted lines show the total 1σ uncertainty in the ephemeris as a function of cycle number.

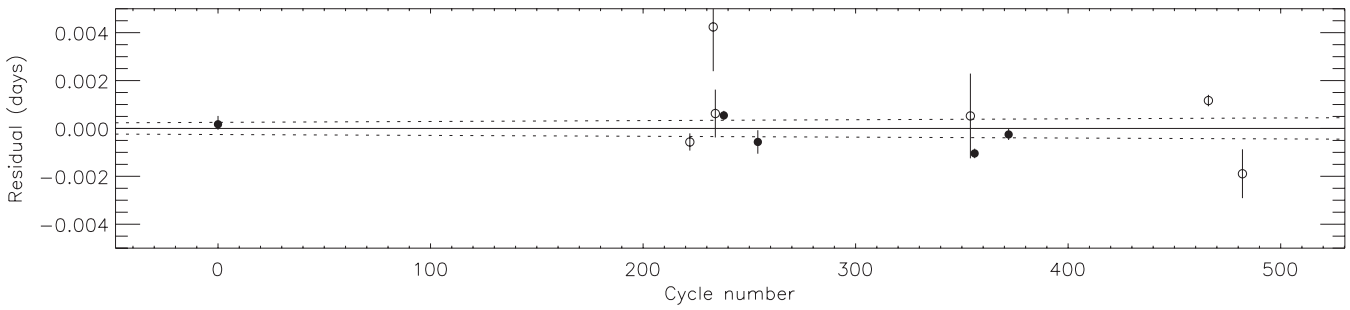

Figure 5. Plot of the residuals of the timings of mid-transit of WASP-16 versus a linear ephemeris. Other comments are the same as for Fig. 4.

Table 3. Parameters of the fit to the light curves of WASP-15 from the JKTEBOP analysis (top). The final parameters are given in bold and the parameters found by other studies are shown (below). Quantities without quoted uncertainties were not given by those authors but have been calculated from other parameters which were.

Source	$r_A + r_b$	k	i (°)	r_A	r_b
GROND g	0.1538 ± 0.0121	0.0967 ± 0.0031	85.56 ± 1.21	0.1403 ± 0.0106	0.01356 ± 0.00137
GROND r	0.1466 ± 0.0065	0.0936 ± 0.0014	86.13 ± 0.72	0.1341 ± 0.0058	0.01255 ± 0.00070
GROND i	0.1505 ± 0.0063	0.0956 ± 0.0013	85.68 ± 0.63	0.1374 ± 0.0057	0.01313 ± 0.00069
GROND z	0.1519 ± 0.0084	0.0959 ± 0.0014	85.51 ± 0.84	0.1386 ± 0.0076	0.01329 ± 0.00080
DFOSC R	0.1545 ± 0.0086	0.0933 ± 0.0023	85.27 ± 0.87	0.1413 ± 0.0078	0.01318 ± 0.00093
Final results	$\mathbf{0.1500 \pm 0.0037}$	$\mathbf{0.09508 \pm 0.00078}$	$\mathbf{85.74 \pm 0.38}$	$\mathbf{0.1370 \pm 0.0033}$	$\mathbf{0.01303 \pm 0.00039}$
West et al. (2009)	0.1436	0.099 ± 0.001		0.1331	0.01318
Triaud et al. (2010)	0.1474	$0.09842^{+0.00067}_{-0.00058}$	$85.96^{+0.29}_{-0.41}$	$0.1342^{+0.0039}_{-00027}$	$0.01321^{+0.00047}_{-0.00030}$

Table 4. Parameters of the fit to the light curves of WASP-16 from the JKTEBOP analysis (top). The final parameters are given in bold and the parameters found by Lister et al. (2009) are shown below. Quantities without quoted uncertainties were not given by Lister et al. (2009) but have been calculated from other parameters which were.

Source	$r_A + r_b$	k	i (°)	r_A	r_b
DFOSC transit 1	0.1365 ± 0.0052	0.1118 ± 0.0060	83.84 ± 0.39	0.1228 ± 0.0053	0.01364 ± 0.00043
DFOSC transit 3	0.1354 ± 0.0073	0.1198 ± 0.0032	84.14 ± 0.59	0.1209 ± 0.0063	0.01448 ± 0.00090
DFOSC transit 4	0.1362 ± 0.0050	0.1204 ± 0.0035	84.09 ± 0.44	0.1216 ± 0.0046	0.01464 ± 0.00063
Euler transit	0.1219 ± 0.0071	0.1074 ± 0.0038	84.75 ± 0.55	0.1101 ± 0.0067	0.01182 ± 0.00059
Final results	$\mathbf{0.1362 \pm 0.0031}$	$\mathbf{0.1190 \pm 0.0022}$	$\mathbf{83.99 \pm 0.26}$	$\mathbf{0.1218 \pm 0.0030}$	$\mathbf{0.01402 \pm 0.00033}$
Lister et al. (2009)	0.1167	$0.1095^{+0.0023}_{-0.0018}$	$85.22^{+0.27}_{-0.43}$	0.1065	0.01012

theoretically predicted values[8] or included as fitted parameters. We made no attempt to fit for both coefficients in the four bi-parametric laws as they are very strongly correlated (Carter et al. 2008; Southworth 2008). The non-linear coefficients were instead perturbed by ± 0.1 on a flat distribution when running the error analysis algorithms, in order to account for their intrinsic uncertainty.

A circular orbit was adopted for both systems as the radial velocities indicate circularity with limits in eccentricity of $e < 0.087$ for WASP-15 (Triaud et al. 2010) and $e < 0.052$ for WASP-16 (Pont et al. 2011). The coefficients of a polynomial function of the out-of-transit magnitude were included when modelling the GROND data, to account for the fact that such a function was used to normalize the data when constructing the differential magnitudes. We checked for correlations between the coefficients of the polynomial and the other parameters of the fit, finding a significant correlation only between k and the quadratic coefficient. The correlation coefficients in this case are in the region of 0.4 for the g band, 0.5 for the r band and 0.65 for the i and z bands, depending on the specifics of how LD was treated. The uncertainties in the resulting parameters induced by this correlation are accounted for in our methods for estimating the parameter uncertainties.

Error bars for the fitted parameters were obtained in two ways: from 1000 Monte Carlo simulations for each solution and via a residual-permutation algorithm (Southworth 2008). The final parameter values are the unweighted mean of those from the solutions involving the four two-parameter LD laws. Their error bars are the larger of the Monte Carlo or residual-permutation alternatives, with an extra contribution to account for variations between solutions with the different LD laws. Tables of individual results for each light curve can be found in the Supplementary Information.

For WASP-15, we found that the residual-permutation method returned moderately larger uncertainties for the g and z light curves, as expected from Fig. 1. We were able to adopt solutions with the linear LD coefficient fitted for the GROND data, but had to use solutions with fixed LD coefficients for the DFOSC observations as they only cover half a transit. The sets of photometric parameters agree extremely well (Table 3) and were combined into a weighted mean after downweighting the DFOSC transit by doubling the parameter error bars. Published results are in acceptable agreement with these weighted mean values.

For WASP-16 the results for the three DFOSC transits agree very well with each other but not with those for the Euler data set (Table 4), which is unsurprising given the best fits plotted in Fig. 3. We therefore combined only the results from the DFOSC transits into a weighted mean to obtain our final photometric parameters. The error bars quoted by Lister et al. (2009) appear to be rather small given the available data and the discrepancy with our follow-up observations.

4 PHYSICAL PROPERTIES

The physical properties of the two systems can be determined from the photometric parameters measured from the light curves, the spectroscopic properties of the host star (velocity amplitude K_A, effective temperature $T_{\rm eff}$ and metallicity $\left[\frac{\rm Fe}{\rm H}\right]$) and constraints from theoretical stellar evolutionary models. We used the approach presented by Southworth (2009), which begins with an estimate of the velocity amplitude of the planet, K_b. A set of physical properties can then be calculated from K_A, K_b, r_A, r_b, i and orbital period using standard formulae. The expected radius and $T_{\rm eff}$ of a star of this mass and $\left[\frac{\rm Fe}{\rm H}\right]$ can then be obtained by interpolating within the

[8] Theoretical LD coefficients were obtained by bilinear interpolation to the host star's $T_{\rm eff}$ and $\log g$ using the JKTLD code available from http://www.astro.keele.ac.uk/jkt/codes/jktld.html.

Table 5. Spectroscopic properties of the host stars in WASP-15 and WASP-16 adopted from the literature and used in the determination of the physical properties of the systems.

Source	WASP-15	Ref.	WASP-16	Ref.
$T_{\rm eff}$ (K)	6405 ± 80	1	5630 ± 70	1
$\left[\frac{\rm Fe}{\rm H}\right]$ (dex)	0.00 ± 0.10	1	0.07 ± 0.10	1
$K_{\rm A}$ (m s^{-1})	64.6 ± 1.2	2	116.7 ± 2.2	3

References: (1) Doyle et al. (2013); (2) Triaud et al. (2010); and (3) Lister et al. (2009).

predictions of theoretical stellar models. The value of $K_{\rm b}$ is then iteratively refined to maximize the match between the observed and predicted $T_{\rm eff}$, and the measured $r_{\rm A}$ and predicted $\frac{R_{\rm A}}{a}$. This procedure is performed over a sequence of ages for the star, beginning at the zero-age main sequence and terminating once it becomes significantly evolved, in order to find the best overall fit and the age of the system.

We determined the physical properties of WASP-15 and WASP-16 using this approach, as implemented in the ABSDIM code (Southworth 2009), and the spectroscopic properties of the stars as summarized in Table 5. We have adopted the atmospheric parameters ($T_{\rm eff}$ and $\left[\frac{\rm Fe}{\rm H}\right]$) from Doyle et al. (2013), as this represents a thorough analysis of observational material of greater quality than for alternative measurements (see Section 1). The statistical errors were propagated through the analysis using a perturbation algorithm (Southworth, Maxted & Smalley 2005), which has the advantage of yielding a complete error budget for every output parameter.

Systematic errors are also incurred through the use of stellar theory to constrain the properties of the host stars; these were assessed by running separate solutions for each of five different sets of stellar model predictions (Claret 2004; Demarque et al. 2004; Pietrinferni et al. 2004; VandenBerg, Bergbusch & Dowler 2006; Dotter et al. 2008) as implemented by Southworth (2010). Finally, a model-independent set of results was generated using an empirical calibration of stellar properties found from well-studied eclipsing binary star systems. The empirical calibration follows the approach introduced by Enoch et al. (2010) but with the improved calibration coefficients derived by Southworth (2011). The individual solutions can be found in Tables A10 and A11 in the Supplementary Information. We used the set of physical constants given by Southworth (2011, their table 3).

Tables 6 and 7 contain our final physical properties for the WASP-15 and WASP-16 systems, plus published measurements for comparison. The mass, radius, surface gravity and density of the star are denoted by $M_{\rm A}$, $R_{\rm A}$, $\log g_{\rm A}$ and $\rho_{\rm A}$, and of the planet by $M_{\rm b}$, $R_{\rm b}$, $g_{\rm b}$ and $\rho_{\rm b}$. $T'_{\rm eq}$ is the equilibrium temperature of the planet (neglecting albedo and heat redistribution) and Θ is the Safronov (1972) number. All quantities with a dependence on stellar theory have separate statistical and systematic error bars quoted. The statistical error bar for a quantity is the largest of the five error bars found in the solutions using different theoretical model predictions. The systematic error bar denotes the largest deviation between the final value of the quantity and the individual values from using the five different sets of models.

The higher $T_{\rm eff}$ adopted for WASP-15 A in the current work caused us to find the star to be more massive and less evolved than previously thought. Our results are in good agreement with previous determinations but are significantly more precise due to the new photometry presented in this paper. Our results for WASP-16 go in the reverse direction: we find a less massive and slightly more evolved star (with a $\log g$ closer to the spectroscopic determination by Doyle et al. 2013). The planet WASP-16 b is $0.21\,R_{\rm Jup}$ (2.5σ) larger than previously thought, leading to a lower surface gravity and density by 2σ. We find an old age of $8.6^{+3.4}_{-2.9}$ Gyr for WASP-16, in agreement with the absence of emission in the calcium H and K lines (B. Smalley, private communication). The measurements for the planetary masses and radii are contrasted in Fig. 6.

5 SUMMARY

WASP-15 and WASP-16 are two TEPs whose discovery was announced by the SuperWASP Consortium in 2009. Since then both have been the subject of follow-up spectroscopic analyses to measure their Rossiter–McLaughlin effects and host star temperatures, but neither have benefited from additional transit photometry to refine measurements of their orbital ephemerides and physical properties. We have rectified this situation by obtaining new light curves of two transits for WASP-15, of which one was covered in four optical passbands simultaneously, and of four transits for WASP-16.

We modelled these photometric data using the JKTEBOP code with careful attention paid to LD and error analysis, and augmented them with published spectroscopic parameters in order to find the physical properties of the components of both systems. Our approach followed that of the *Homogeneous Studies* project by the first

Table 6. Derived physical properties of the WASP-15 system and a comparison to previous measurements. Separate statistical and systematic error bars are given for the results from the current work.

	This work	West et al. (2009)	Triaud et al. (2010)	Doyle et al. (2013)
$M_{\rm A}$ ($M_\odot$)	$1.305 \pm 0.051 \pm 0.006$	1.18 ± 0.12	$1.18^{+0.14}_{-0.12}$	1.23 ± 0.09
$R_{\rm A}$ ($R_\odot$)	$1.522 \pm 0.044 \pm 0.002$	1.477 ± 0.072	$1.440^{+0.064}_{-0.057}$	1.15 ± 0.16
$\log g_{\rm A}$ (CGS)	$4.189 \pm 0.021 \pm 0.001$	4.169 ± 0.033		
$\rho_{\rm A}$ ($\rho_\odot$)	0.370 ± 0.027	0.365 ± 0.037	$0.394^{+0.024}_{-0.032}$	
$M_{\rm b}$ ($M_{\rm Jup}$)	$0.592 \pm 0.019 \pm 0.002$	0.542 ± 0.050	$0.551^{+0.041}_{-0.038}$	
$R_{\rm b}$ ($R_{\rm Jup}$)	$1.408 \pm 0.046 \pm 0.002$	1.428 ± 0.077	$1.379^{+0.067}_{-0.058}$	
$g_{\rm b}$ (m s^{-2})	7.39 ± 0.46	6.08 ± 0.62		
$\rho_{\rm b}$ ($\rho_{\rm Jup}$)	$0.198 \pm 0.018 \pm 0.000$	0.186 ± 0.026		
$T'_{\rm eq}$ (K)	1676 ± 29	1652 ± 28		
Θ	$0.0332 \pm 0.0013 \pm 0.0001$			
a (au)	$0.05165 \pm 0.00067 \pm 0.00008$	0.0499 ± 0.0018	$0.0499^{+0.0019}_{-0.0017}$	
Age (Gyr)	$2.4\,^{+0.6\ +0.2}_{-0.6\ -0.4}$	$3.9^{+2.8}_{-1.3}$		

Table 7. Derived physical properties of the WASP-16 system and a comparison to previous measurements. Separate statistical and systematic error bars are given for the results from the current work.

	This work	Lister et al. (2009)	Doyle et al. (2013)
M_A ($M_\odot$)	$0.980 \pm 0.049 \pm 0.023$	$1.022^{+0.074}_{-0.129}$	1.09 ± 0.09
R_A ($R_\odot$)	$1.087 \pm 0.041 \pm 0.008$	$0.946^{+0.057}_{-0.052}$	1.34 ± 0.20
$\log g_A$ (CGS)	$4.357 \pm 0.022 \pm 0.003$	$4.495^{+0.030}_{-0.054}$	
ρ_A ($\rho_\odot$)	0.762 ± 0.056	$1.21^{+0.13}_{-0.18}$	
M_b (M_{Jup})	$0.832 \pm 0.036 \pm 0.013 \pm 0.855^{+0.043}_{-0.076}$		
R_b (R_{Jup})	$1.218 \pm 0.039 \pm 0.009$	$1.008^{+0.083}_{-0.060}$	
g_b (m s^{-2})	13.92 ± 0.71	$19.2^{+1.9}_{-2.6}$	
ρ_b (ρ_{Jup})	$0.431 \pm 0.033 \pm 0.003$	$0.83^{+0.13}_{-0.17}$	
T'_{eq} (K)	1389 ± 24	1280^{+35}_{-21}	
Θ	$0.0579 \pm 0.0021 \pm 0.0004$	0.070 ± 0.010	
a (au)	$0.04150 \pm 0.00070 \pm 0.00032$	$0.0421^{+0.0010}_{-0.0018}$	
Age (Gyr)	$8.6^{+3.3\ +0.6}_{-2.7\ -0.9}$	$2.3^{+5.8}_{-2.2}$	

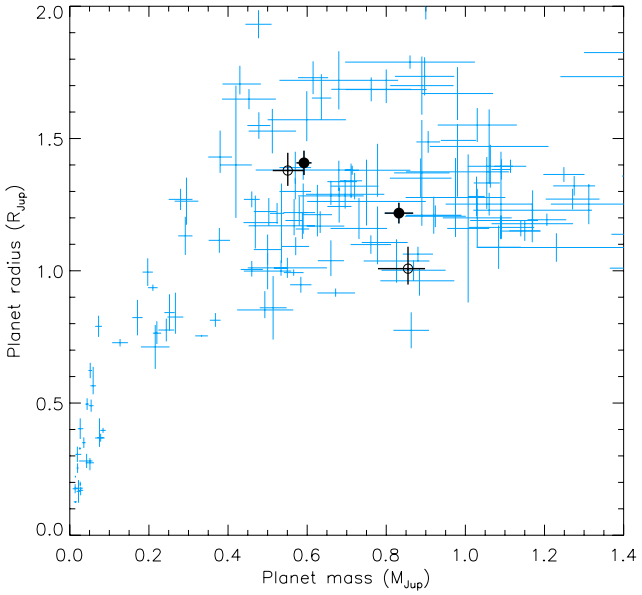

Figure 6. Plot of planet radii versus their masses. The overall population of planets is shown using blue crosses, using data taken from TEPCat on 2013 February 11. WASP-15 b and WASP-16 b are indicated using black lines with open circles for the values from their respective discovery papers and filled circles for the new results from the current work. The outlier with a mass of 0.86 M_{Jup} but with a radius of only 0.78 R_{Jup} is the recently discovered system WASP-59 (Hébrard et al. 2013).

author, and WASP-15 and WASP-16 have been added to the Transiting Extrasolar Planet Catalogue.[9]

We confirm that WASP-15 is a highly inflated planet with a large atmospheric scale height which, when combined with the brightness of its host star ($V = 10.92$), makes it a good candidate for studying the atmospheres of extrasolar planets. Our simultaneous observations in four optical passbands are in principle good for probing this, so we attempted to do so using the methods of Southworth et al. (2012a). In practice, we found that our data are not extensive enough to allow inferences to be drawn. This is in line with previous experience (Mancini et al. 2013a,b; Nikolov et al. 2013) and could be rectified by obtaining new observations with GROND.

We find a significantly larger radius for WASP-16 b, moving it from the edge of the mass–radius distribution to an area of parameter space more typical for transiting hot Jupiters. This underlines the point that multiple high-quality transit light curves are needed for the physical properties of a TEP to be reliably constrained. The detailed error budgets we have calculated show a typical situation: an improved understanding of both WASP-15 and WASP-16 would require additional transit light curves, radial-velocity observations and more precise $\left[\frac{Fe}{H}\right]$ determinations.

[9] The Transiting Extrasolar Planet Catalogue (TEPCat) is available at http://www.astro.keele.ac.uk/jkt/tepcat/.

ACKNOWLEDGEMENTS

This paper incorporates observations collected at the MPG/ESO 2.2 m telescope located at ESO La Silla, Chile. Operations of this telescope are jointly performed by the Max Planck Gesellschaft and the European Southern Observatory. GROND has been built by the high-energy group of MPE in collaboration with the LSW Tautenburg and ESO, and is operated as a PI-instrument at the 2.2 m telescope. We thank Timo Anguita and Régis Lachaume for technical assistance during the observations. The operation of the Danish 1.54 m telescope is financed by a grant to UGJ from the Danish Natural Science Research Council. The reduced light curves presented in this work will be made available at the CDS (http://vizier.u-strasbg.fr/) and at http://www.astro.keele.ac.uk/∼jkt/. J Southworth acknowledges the financial support from STFC in the form of an Advanced Fellowship. The research leading to these results has received funding from the European Community's Seventh Framework Programme (FP7/2007-2013/) under grant agreement Nos. 229517 and 268421. Funding for the Stellar Astrophysics Centre (SAC) is provided by The Danish National Research Foundation. KAA, MD, MH, CL and CS are thankful to Qatar National Research Fund (QNRF), member of Qatar Foundation, for support by grant NPRP 09-476-1-078. TCH acknowledges the financial support from the Korea Research Council for Fundamental Science and Technology (KRCF) through the Young Research Scientist Fellowship Programme and is supported by the KASI (Korea Astronomy and Space Science Institute) grant 2012-1-410-02/2013-9-400-00. S-HG and X-SF acknowledge the support from NSFC under the grant No. 10873031. The research is supported by the ASTERISK project (ASTERoseismic Investigations with SONG and

Kepler) funded by the European Research Council (grant agreement No. 267864). FF (ARC), OW (FNRS research fellow) and J Surdej acknowledges the support from the Communauté française de Belgique – Actions de recherche concertées – Académie Wallonie-Europe. The following internet-based resources were used in research for this paper: the ESO Digitized Sky Survey; the NASA Astrophysics Data System; the SIMBAD data base operated at CDS, Strasbourg, France; and the arXiv scientific paper preprint service operated by Cornell University.

REFERENCES

Albrecht S. et al., 2012, ApJ, 757, 18
Blackwell D. E., Petford A. D., Shallis M. J., 1980, A&A, 82, 249
Brown D. J. A. et al., 2012, MNRAS, 423, 1503
Carter J. A., Yee J. C., Eastman J., Gaudi B. S., Winn J. N., 2008, ApJ, 689, 499
Claret A., 2004, A&A, 424, 919
Demarque P., Woo J.-H., Kim Y.-C., Yi S. K., 2004, ApJS, 155, 667
Dotter A., Chaboyer B., Jevremović D., Kostov V., Baron E., Ferguson J. W., 2008, ApJS, 178, 89
Doyle A. P. et al., 2013, MNRAS, 428, 3164
Eastman J., Siverd R., Gaudi B. S., 2010, PASP, 122, 935
Enoch B., Collier Cameron A., Parley N. R., Hebb L., 2010, A&A, 516, A33
Hébrard G. et al., 2013, A&A, 549, A134
Lister T. A. et al., 2009, ApJ, 703, 752
Mancini L. et al., 2013a, A&A, 551, A11
Mancini L. et al., 2013b, MNRAS, 430, 2932
Maxted P. F. L., Koen C., Smalley B., 2011, MNRAS, 418, 1039
Nikolov N., Chen G., Fortney J., Mancini L., Southworth J., van Boekel R., Henning T., 2013, A&A, 553, A26
Pietrinferni A., Cassisi S., Salaris M., Castelli F., 2004, ApJ, 612, 168
Pont F., Husnoo N., Mazeh T., Fabrycky D., 2011, MNRAS, 414, 1278
Safronov V. S., 1972, Evolution of the Protoplanetary Cloud and Formation of the Earth and Planets. Israel Program for Scientific Translation, Jerusalem
Southworth J., 2008, MNRAS, 386, 1644
Southworth J., 2009, MNRAS, 394, 272
Southworth J., 2010, MNRAS, 408, 1689
Southworth J., 2011, MNRAS, 417, 2166
Southworth J., 2012, MNRAS, 426, 1291
Southworth J., Maxted P. F. L., Smalley B., 2004, MNRAS, 349, 547
Southworth J., Maxted P. F. L., Smalley B., 2005, A&A, 429, 645
Southworth J. et al., 2009a, MNRAS, 396, 1023
Southworth J. et al., 2009b, ApJ, 707, 167
Southworth J., Mancini L., Maxted P. F. L., Bruni I., Tregloan-Reed J., Barbieri M., Ruocco N., Wheatley P. J., 2012a, MNRAS, 422, 3099
Southworth J. et al., 2012b, MNRAS, 426, 1338
Stetson P. B., 1987, PASP, 99, 191
Tregloan-Reed J., Southworth J., 2012, MNRAS, 431, 966
Triaud A. H. M. J., 2011, A&A, 534, L6
Triaud A. H. M. J. et al., 2010, A&A, 524, A25
VandenBerg D. A., Bergbusch P. A., Dowler P. D., 2006, ApJS, 162, 375
West R. G. et al., 2009, AJ, 137, 4834
Winn J. N., Fabrycky D., Albrecht S., Johnson J. A., 2010, ApJ, 718, L145

SUPPORTING INFORMATION

Additional Supporting Information may be found in the online version of this article:

Appendix A. Full results for the light curves analysed in this work (http://mnras.oxfordjournals.org/lookup/suppl/doi:10.1093/mnras/stt1089/-/DC1).

Please note: Oxford University Press is not responsible for the content or functionality of any supporting materials supplied by the authors. Any queries (other than missing material) should be directed to the corresponding author for the paper.

This paper has been typeset from a TEX/LATEX file prepared by the author.